Calcium channel levels at single synapses predict release probability and are upregulated in homeostatic potentiation

Scott J. Gratz[1], Joseph J. Bruckner[2], Roberto Hernandez[3], Karam Khateeb[4], Gregory T. Macleod[3], and Kate M. O'Connor-Giles[1,4*]

[1] Laboratory of Cell and Molecular Biology, University of Wisconsin-Madison, Madison, WI 53706

[2] Present address: Institute of Neuroscience, University of Oregon, Eugene, OR 97401

[3] Department of Biological Sciences and Wilkes Honors College, Florida Atlantic University, Jupiter, FL 33458, USA

[4] Laboratory of Genetics, University of Wisconsin-Madison, Madison, WI 53706

*For correspondence: Kate M. O'Connor-Giles, 227D Robert M. Bock Labs, 1525 Linden Dr., Madison, WI 53706. email: oconnorgiles@wisc.edu

The authors declare that no competing interests exist.

Abstract

Communication in neural circuits depends on neurotransmitter release at specialized domains of presynaptic terminals called active zones. Evidence in multiple systems indicates that neurotransmitter release properties vary significantly, even between neighboring active zones of the same neuron. To investigate the role of voltage-gated calcium channels in determining diverse release properties, we combined endogenous tagging of the Ca_V2 channel Cacophony with functional imaging at *Drosophila* neuromuscular junctions. We find that calcium channels are differentially localized to active zones and robustly predict release probability at single synapses. Synaptic calcium channel levels, in turn, are highly correlated with ELKS/Bruchpilot levels at the active zone cytomatrix. During acute homeostatic potentiation, active zone cytomatrix remodeling is accompanied by a rapid increase in calcium channel levels. We propose that dynamic reorganization of the active zone cytomatrix during short-term plasticity generates new sites for the incorporation of calcium channels to modulate release properties and circuit function.

Introduction

Neurotransmitter release properties at individual synapses play an important role in defining information flow within neural circuits and establishing how circuits can be modified in response to experience. Neurotransmitter release occurs at specialized domains of presynaptic membranes called active zones. Release properties, which vary significantly within neuronal subtypes and single neurons, are determined locally at individual active zones, raising the question of how this complex organization is achieved (Atwood and Karunanithi, 2002; Branco and Staras, 2009; Hatt and Smith, 1976).

A conserved complex of active zone-associated proteins makes up the active zone cytomatrix (Ackermann et al., 2015). In *Drosophila*, these proteins include Liprin-α, Syd-1, the ELKS-family protein Bruchpilot (Brp), the Rab3-interacting molecule RIM, Piccolo-RIM related Fife, RIM-binding protein, and Unc13 (Bohme et al., 2016; Bruckner et al., 2012; Bruckner et al., 2017; Graf et al., 2012; Kittel et al., 2006; Liu et al., 2011; Muller et al., 2012; Owald et al., 2010). Active zone cytomatrix proteins contain protein-binding domains that mediate numerous interactions with other cytomatrix proteins, synaptic vesicle-associated proteins, and/or calcium channels. Genetic studies in *Drosophila*, *C. elegans*, and mice have revealed multifaceted roles for proteins of the active zone cytomatrix in organizing presynaptic terminals to promote high-probability neurotransmitter release. Thus, a common complex of proteins establishes the fundamental organization of active zones required to support robust synaptic communication. However, due in large part to limits on the ability to interrogate molecular and structural arrangements at single synapses of known function, it is not understood how these common building blocks are differentially deployed to establish synapses with distinct properties or modulate release properties during synaptic plasticity.

The *Drosophila* neuromuscular junction (NMJ) provides an ideal model for investigating the molecular underpinnings of distinct synaptic release properties *in vivo*. Glutamatergic motorneurons form hundreds of synapses with their postsynaptic muscle targets. These synapses have many presynaptic parallels to excitatory synapses in the mammalian CNS, including molecular composition, ultrastructural organization of active zones, and neurotransmitter release parameters (Ackermann et al., 2015; Harris and Littleton, 2015; Petzoldt et al., 2016; Zhan et al., 2016). Functional imaging studies with genetically encoded calcium indicators have facilitated the investigation of neurotransmission at single synapses of *Drosophila* motorneurons, revealing great heterogeneity in release properties between active zones (Guerrero et al., 2005; Melom et al., 2013; Peled and Isacoff, 2011; Peled et al., 2014). Notably, this functional heterogeneity is observed within single motorneurons and motorneuron branches forming synapses with single postsynaptic muscles, enabling the focused investigation of local presynaptic determinants of diverse synaptic strengths.

Here, we engineered *Drosophila* to incorporate a fluorescent tag in all endogenous forms of *cacophony (cac),* which encodes the pore-forming subunit of the sole calcium channel required for triggering neurotransmitter release at *Drosophila* synapses. We find that synaptic Cac levels vary significantly and reliably predict neurotransmitter release probability at individual active zones of single motor neurons. Calcium channel levels are strongly correlated with the amount of ELKS/Brp at the active zone cytomatrix. During acute homeostatic potentiation, calcium channel levels are rapidly increased as the active zone cytomatrix is remodeled to support increased neurotransmitter release. These findings suggest that functional diversity rests on heterogeneous calcium channel levels established by the active zone cytomatrix, and define calcium channel clustering at active zones as a target for rapid modification during short-term synaptic plasticity.

Results

Endogenous tagging of the Cacophony Ca_V2 calcium channel

cac encodes the only *Drosophila* Ca_V2-family member and is homologous to mammalian N- and P/Q-type voltage-gated calcium channels. To date, studies in *Drosophila* have employed a C-terminally tagged transgene, UAS-Cac-GFP, to assess calcium channel localization – an approach that has enabled the identification of multiple regulators of calcium channel localization to active zones (Kawasaki et al., 2004). However, use of the transgene has several drawbacks that limit its utility for investigating the molecular underpinnings of diverse release parameters: (1) *cac* is expressed, generally at high levels, under the control of Gal4 instead of endogenous regulatory elements; (2) only one of 15 *cac* isoforms is expressed and RNA editing, a conserved mechanism for regulating ion channel function, is likely completely absent; (3) the C-terminal position of GFP obstructs a conserved PDZ-binding domain that mediates interactions with synaptic proteins; and (4) expression of the single Cac isoform was shown to rescue viability, but not flight, in null alleles, indicating channel function is not fully restored (Kawasaki et al., 2002; Kawasaki et al., 2004). To overcome these limitations and create a reagent for following all endogenous Ca_V2 channels *in vivo*, we targeted the translational start site of 14 out of 15 *cac* isoforms for CRISPR-mediated incorporation of superfolder GFP (sfGFP) (Figure 1A). This location also results in the in-frame translation of sfGFP within the longer N-terminal cytoplasmic domain of the

single isoform (isoform N) with an earlier start site, allowing us to follow the full complement of endogenous Cac channels (Figure 1B).

Across phyla, neurotransmitter release depends on the synaptic localization of Ca_v2 channels, and previous studies with UAS-Cac-GFP demonstrate that tagged channels accumulate at synapses upon neuronal expression (Kawasaki et al., 2004). Consistently, we find that $Cac^{sfGFP-N}$ specifically localizes to presynaptic terminals marked by the active zone cytomatrix protein Brp at larval NMJs (Figure 1C). We also observe synaptic localization in the larval ventral ganglion and the adult brain (Figure 1D,E). In the adult brain, it is immediately apparent that endogenous Cac levels vary between different brain regions. Most notably, we consistently observe higher channel levels in the mushroom body, presumably reflecting a functional requirement for higher channel numbers coupled with differential regulation of channel transcription, translation and/or trafficking to synapses.

Endogenously tagged Cacophony functions normally *in vivo*

$cac^{sfGFP-N}$ flies are homozygous and hemizygous viable, emerge at expected frequencies, and are capable of effective flight. To directly evaluate the function of endogenously tagged channels, we assayed presynaptic calcium influx via fluorescence imaging of a calcium-sensitive dye loaded into axon terminals *in situ* (Macleod, 2012). The use of a rapid-binding chemical dye loaded in constant proportion to a calcium-insensitive dye provided ratiometric resolution of single action potential-mediated calcium transients and allowed for direct comparisons between terminal types, preparations, and genotypes (Figure 2A,B) (Lu et al., 2016). The resting level of calcium is no different between *$cac^{sfGFP-N}$* and wild-type larvae in either type-Ib (big) or -Is (small) terminals on muscle fiber 6 (Figure 2C). Similarly, the amplitude of the single action potential-mediated calcium transient does not differ between the two genotypes (Figure 2D). Finally, the amplitude of the calcium plateau during trains of action potentials is independent of both endogenous calcium binding and dye loading, and this too is no different between *$cac^{sfGFP-N}$* and wild type (Figure 2E). Thus, endogenously tagged calcium channels exhibit normal calcium influx.

We next evaluated synaptic transmission in *$cac^{sfGFP-N}$* through intracellular recordings at the NMJ. We found no differences between control and either genotype in mEJP frequency and amplitude, EJP amplitude, and quantal content, consistent with the observation of normal Ca^{2+} influx (Figure 2F-J). In addition to its role in neurotransmission, Cac has an established role in promoting synapse formation (Rieckhof et al., 2003). We assessed bouton number at NMJ6/7 and found a 12% decrease in bouton number at NMJ6/7 in *$cac^{sfGFP-N}$* animals (Figure 2—figure supplement 1A-C). At NMJ4, there is no difference in bouton number between *$cac^{sfGFP-N}$* and wild type (Figure 2—figure supplement 1A,B,D). Similarly, active zone number per bouton is unaltered at *$cac^{sfGFP-N}$* NMJs (Figure 2—figure supplement 1E). Together these analyses indicate that the incorporation of a fluorescent tag into the endogenous protein leaves channel function substantively intact *in vivo*.

Calcium channel levels differ at individual active zones of single neurons

The probability that an action potential will elicit release of a synaptic vesicle at an individual synapse (synaptic probability of release, P_r) is determined by the number of readily releasable synaptic vesicles (N) and their individual probability of release (P_v), which is heavily influenced by the number and organization of presynaptic calcium channels. The striking differences in synaptic calcium channel levels between distinct regions of the adult brain prompted us to investigate the role of differential calcium channel clustering in release heterogeneity between individual synapses. To assess whether calcium channel number differs between individual active zones of single neurons, we turned to the NMJ where we can separately evaluate Cac levels at hundreds of individual synapses formed between a single motorneuron and post-synaptic muscle cell. Using Brp to independently delineate individual presynaptic active zones, we find that total Cac levels vary considerably between synapses formed by a single RP3 motorneuron branch, with most active zones exhibiting low-to-moderate levels and a smaller number expressing high Cac levels (Figure 3A,B). Because the size of Brp puncta are near the light-level limit of resolution, active zones with very high levels of Cac could in fact be multiple closely spaced active zones (Ehmann et al., 2014). To overcome this caveat, we measured peak intensity per puncta, and observe a similar distribution (Figure 3C).

Calcium channel levels predict release probability at single active zones

The observation that calcium channel clustering varies significantly between active zones of single neurons highlights the importance of methods that enable the evaluation of individual active zones for understanding the molecular and structural features that establish and tune synaptic release properties. Functional imaging studies employing GCaMP targeted to postsynaptic densities have been used to optically monitor release at *Drosophila* NMJs via calcium influx through postsynaptic glutamate receptors (Guerrero et al., 2005; Melom et al., 2013; Peled and Isacoff, 2011; Peled et al., 2014). These studies have revealed significant functional heterogeneity between individual synapses of motorneuron-muscle pairs, with the majority of active zones exhibiting low probability of release (P_r) and a

small minority highly active – reminiscent of the distribution we observe for calcium channel levels (Guerrero et al., 2005; Melom et al., 2013; Peled and Isacoff, 2011; Peled et al., 2014).

To directly assess a link between calcium channel levels and neurotransmitter release properties at single active zones, we replaced sfGFP in the endogenous *cac* locus with sequence encoding the slow-bleaching, monomeric red-shifted fluorophore TagRFP and expressed postsynaptically targeted GCaMP5 under the control of a muscle promoter (PS-GCaMP) in $cac^{TagRFP\text{-}N}$ flies. We monitored neurotransmission in semi-intact larval preparations in hemolymph-like solution (HL6) containing 1.5 mM external calcium during 1-Hz stimulation (Video 1). To map postsynaptic calcium transients to presynaptic active zones, we localized each calcium influx event to a region of interest (ROI) defined by local ΔF/F maxima, then used nearest neighbor analysis to assign each event to the closest active zone defined by the center of mass of each $Cac^{TagRFP\text{-}N}$-positive punctum (Figure 4—figure supplement 1A-E; see 'Materials and methods' for details). We compared manual and automated approaches for identifying ROIs and observed minimal differences between the two (Figure 4—figure supplement 1F). Because the manual method was more robust to noise in the data, we proceeded with this approach.

To calculate synaptic P_r, we quantified the number of times a vesicle was released in response to 100 stimuli at individual active zones of motorneuron RP3 synapsing with muscle 6 (Figure 4A,B). We observe significant heterogeneity in release probability, with a positively skewed distribution that mirrors previous observations (Figure 4—figure supplement 1G) (Melom et al., 2013; Peled et al., 2014). Our results agree with prior studies in which release sites were inferred based on the delineation of ROIs defined by postsynaptic GCaMP, indicating the robustness of both approaches (Melom et al., 2013; Peled and Isacoff, 2011; Peled et al., 2014). Similar to these studies, we found that ~90% of active zones had release probabilities between 0.01 and .5, with a median P_r of .11, which corresponds remarkably well with physiological and prior optical imaging measurements (Lu et al., 2016; Newman et al., 2017). Our approach also allowed us to readily identify functionally silent synapses, which accounted for 8% of active zones analyzed. This number is somewhat smaller than estimates from a prior study, which found that ~20% of sites that released vesicles spontaneously did not participate in evoked release (Melom et al., 2013). As these studies were conducted at different NMJs, this difference may reflect biological differences between motorneurons. Finally, we observed a small number of sites with release probability as high as 93%. However, we cannot rule out the possibility that these rates reflect summed release from two closely spaced active zones.

We next compared peak Cac levels to release probability at each active zone to investigate the relationship between calcium channel number and P_r at individual active zones (Figure 4C). We observe a robust correlation between Cac intensity and P_r at active zones of different strengths (Figure 4D,E). These data are consistent with the conclusion that heterogeneity in calcium channel levels at individual active zones plays a key role in defining diverse synaptic strengths.

Bruchpilot levels correlate with calcium channel levels at single active zones

How might calcium channel levels be determined locally at synapses? A prevailing hypothesis posits the existence of a set number of 'slots' for calcium channels at active zone membranes (Cao et al., 2004). As large scaffolding proteins thought to structurally organize active zones through numerous physical interactions, proteins of the active zone cytomatrix are promising candidates for the establishment of calcium channel slots. Loss-of-function studies in flies and mice, which reveal diminished active zone accumulation of calcium channels in the absence of Brp, RIM-binding protein, RIM, or Fife, provide strong support for this hypothesis (Bruckner et al., 2017; Frank et al., 2010; Graf et al., 2009; Graf et al., 2012; Kaeser et al., 2011; Kittel et al., 2006; Liu et al., 2011; Muller et al., 2012).

To investigate the relationship between the active zone cytomatrix and Cac at the level of single synapses, we used antibodies against Brp to examine the correlation between Brp and endogenous Cac levels as loss of Brp appears to have the most profound effect on mean synaptic levels of transgenically expressed Cac-GFP, resulting in an ~50% reduction (Kittel et al., 2006). We noted that, like Cac, Brp levels vary between individual active zones of single motor terminals with a subset expressing high levels while the remainder express low or moderate levels (Figure 5A). At the level of individual active zones, we find that there is a remarkably high correlation between peak levels of Cac and Brp (Figure 5B,C). An even stronger correlation is observed for total active zone levels of Cac and Brp (r= 0.96, n=12 NMJs from 4 animals). This finding builds on loss-of-function studies to support the model that the active zone cytomatrix establishes synapses with diverse release properties in part by creating sites for calcium channel incorporation at the active zone membrane.

Calcium channel levels are rapidly increased during homeostatic potentiation

Presynaptic homeostatic potentiation is a conserved mechanism for maintaining neural communication within an established range (Cull-Candy et al., 1980).

At the *Drosophila* NMJ, pharmacological inhibition of neurotransmitter receptors by the wasp venom philanthotoxin (PhTx) leads to a compensatory increase in neurotransmitter release within 10 minutes that precisely offsets the postsynaptic deficit (Frank et al., 2006). Detailed mechanistic studies reveal that increases in both the size of the readily-releasable pool of synaptic vesicles and calcium influx underlie increased P_r. However, it remains unknown if the regulation of calcium influx occurs at the level of channel gating properties, channel number, or both (Davis and Muller, 2015; Frank, 2014). Active zone cytomatrix proteins RIM, RIM-binding protein, and Fife are all required for presynaptic homeostasis suggesting the cytomatrix is rapidly mobilized to support increased P_r (Bruckner et al., 2017; Muller et al., 2015; Muller et al., 2012). In a landmark study, Weyhersmuller and colleagues found that active zone levels of Brp are significantly increased within minutes during PhTx-induced presynaptic potentiation (Weyhersmuller et al., 2011). The concomitant increase in release-ready vesicle number led to the model that acute homeostatic challenge induces a rapid reorganization of the active zone cytomatrix to recruit release-ready vesicles.

Given the strong correlation between Brp and calcium channel levels at individual active zones and the established developmental role for active zone cytomatrix proteins in promoting calcium channel accumulation, we sought to determine if calcium channel levels are also regulated on short timescales to support acute homeostatic potentiation. We first confirmed that PhTx-induced presynaptic homeostatic potentiation occurs normally in $cac^{sfGFP\text{-}N}$ larvae (Figure 6—figure supplement 1), enabling us to directly test the hypothesis that calcium channel levels are targets for rapid regulation during acute homeostasis. We treated partially dissected $cac^{sfGFP\text{-}N}$ larvae with nonsaturating concentrations of PhTx for 10 minutes. Immediately following PhTx treatment, preparations were fully dissected, fixed, and stained for GFP and Brp at RP3 motorneurons. Consistent with prior observations, we observe a significant increase in peak Brp levels across active zones (Figure 6A,B). Strikingly, we observe a similar increase in Cac levels, indicating a temporally coordinated correspondence between Brp and Cac accumulation during presynaptic potentiation (Figure 6A,B). We observe a significant rightward shift in the distributions of both peak Bruchpilot and Cac, indicating that active zones are dynamic structures that can rapidly grow beyond the range observed at baseline to accommodate further increases in molecular content (Figure 6C-E). Investigation of total active zone fluorescence following PhTx-induced homeostasis yields similar conclusions (Figure 6—figure supplement 2). Thus, we conclude that the expansion of the active zone cytomatrix during short-term plasticity generates new sites for incorporation of calcium channels as well as release-ready vesicles to rapidly modulate release properties and circuit function (Figure 7).

Discussion

To investigate the role of calcium channel clustering in the establishment and modification of distinct neurotransmitter release properties at single synapses, we incorporated sequences encoding fluorescent tags into the endogenous *cac* locus. We find that Cac is distributed unequally across individual active zones of single motorneurons, and that synaptic Ca_v2 channel levels predict release probability. Brp levels, in turn, predict Cac levels, consistent with the model that the active zone cytomatrix generates slots for calcium channels at the presynaptic membrane. Finally, we find that Cac levels are rapidly increased in concert with Brp during short-term presynaptic homeostatic challenge. Together, these findings indicate that diversity in calcium channel number underlies heterogeneous release properties and define calcium channel levels as a target for rapid modification during short-term synaptic plasticity (Figure 7).

Heterogeneous synaptic calcium channel levels and functional diversity

Diverse synaptic release properties enable complex communication and broaden the capacity of circuits to respond to distinct and changing inputs. Understanding the source of distinct release properties has been of interest since Del Castillo and Katz first proposed the possibility that "some synaptic units respond more readily than others" (Del Castillo and Katz, 1954). Together, the number of release-ready vesicles, N, and their individual release probabilities, P_v, determine synaptic P_r. Because synaptic vesicles fuse in response to a rise in calcium in the microdomain around voltage-gated calcium channels, a major determinant of P_v is the distance between the vesicle and calcium channels. Thus, the number and topographical organization of calcium channels are expected to critically influence P_v.

A lack of reagents and approaches for monitoring endogenous calcium channel numbers and localization at single active zones of known function has hindered progress in understanding their role in defining diverse functional properties. To bridge that gap and generate a reagent for monitoring endogenous calcium channels at well-studied *Drosophila* synapses, we engineered the incorporation of a fluorescent tag into the *cac* locus and confirmed tagged channel function *in vivo* (Figures 1, 2). In the adult brain, we observed striking differences in Cac levels, with mushroom bodies exhibiting particularly high levels. In larvae, we found that calcium channels are distributed heterogeneously between active zones of single motorneurons, with the majority exhibiting low-to-moderate levels and a minority exhibiting high levels (Figure 3). Because active zones, which we

defined using Brp as a co-label, are approximately 200 nm in diameter and, thus, near the resolution of light-level imaging, we cannot exclude the possibility of mistaking two closely spaced active zones for a single large active zone with high total levels of Cac. To reduce this possibility, we focused our analysis on peak Cac levels per puncta, which is less likely than total active zone levels to be inflated in this scenario, and observed similar heterogeneity.

Our observations are consistent with freeze-fracture/immunogold electron microscopy experiments, which report clusters of Ca_V2 channels that vary in size between active zones (Holderith et al., 2012; Indriati et al., 2013; Nakamura et al., 2015; Propst and Ko, 1987). The conclusion that calcium channel levels are differentially distributed between active zones is further supported by the widespread observation of significant heterogeneity in calcium influx at mammalian, frog, and invertebrate synapses (Brenowitz and Regehr, 2007; Ermolyuk et al., 2012; Pawson and Grinnell, 1984; Sheng et al., 2012; Xu-Friedman et al., 2001).

To investigate how diverse calcium channel levels influence release parameters, we combined endogenously tagged Cac with postsynaptically targeted genetically encoded calcium indicators that report neurotransmitter release at the level of individual synapses. In agreement with prior studies at the *Drosophila* NMJ, we observe significant heterogeneity in release probability at individual active zones (Figure 4) (Melom et al., 2013; Newman et al., 2017; Peled et al., 2014). Using automated and manual approaches, which showed strong agreement (Figure 4—figure supplement 1), we identified and mapped quantal release events to individual active zones allowing us to directly assess the relationship between Cac levels and P_r. This analysis revealed a very strong correlation between Ca_V2 calcium channel clustering and P_r at individual active zones of single motor axon branches (Figure 4). We used a strict nearest-neighbor assignment of postsynaptic events to Cac-defined active zones. While this approach successfully removed any ambiguity in assigning events, it may have resulted in the misassignment of a small subset of events, particularly in cases where two or more high-Cac active zones were in close proximity. Although this may have a small effect on the absolute number of release events from some active zones, our data clearly demonstrate that Cac levels are highly predictive of single active zone release probability.

Sheng and colleagues came to a similar conclusion using cell-attached current and capacitance recordings conducted predominantly at single active zones of the rat calyx of Held, one of the largest synapses in the mammalian CNS. Calcium channel numbers per active zone varied between 5 and 218 and strongly correlated with P_r (Sheng et al., 2012). Together, these studies suggest that differences in the number of calcium channels between individual active zones are a conserved determinant of heterogeneous presynaptic release properties. Modeling studies support this conclusion (Homan et al., 2017; Keller et al., 2015; Meinrenken et al., 2002; Nakamura et al., 2015). Of particular note is a recent study that incorporated data obtained from freeze-fracture replica immunogold labeling of $Ca_V2.1$ channels and electrophysiological measurements at the calyx of Held to arrive at a 'perimeter' model in which release-ready synaptic vesicles surround calcium channel clusters that vary in size between active zones (Nakamura et al., 2015). In this model, variability in the number of calcium channels in a cluster establishes heterogeneous synaptic release probabilities by modulating channel-vesicle coupling distances and, thus, P_v.

Rapid active zone reorganization and calcium channel accumulation

Given their central role in regulating P_r, calcium channel clustering appears to be an optimal target for presynaptic plasticity. Indeed, we have found that recruitment of new calcium channels underlies acute presynaptic homeostatic potentiation induced by PhTx inhibition of glutamate receptors (Figure 6). This finding fits well with our current understanding of presynaptic homeostatic potentiation, in which both the size of the readily releasable vesicle pool and calcium influx are increased to potentiate release probability (Davis and Muller, 2015; Frank, 2014). It has remained an open question whether potentiation of calcium influx is achieved through the regulation of calcium channel number, channel gating properties, or a combination of the two. The finding that epithelial sodium channels are required for presynaptic homeostatic potentiation led to the model that these channels modulate membrane potential to increase calcium influx through Cac channels (Younger et al., 2013). Another recent study found that the α2δ calcium channel subunit is required for presynaptic homeostatic potentiation (Wang et al., 2016). While a role in regulating calcium channel levels during potentiation was not investigated, it was proposed that α2δ regulates an increase in readily releasable vesicles during potentiation. Prior studies in flies and mammals demonstrate a role for α2δ in calcium channel clustering, raising the intriguing possibility that α2δ might function during potentiation to promote channel accumulation, which in turn may play a role in enhancing the size of the readily releasable vesicle pool by increasing the number of vesicles that can be positioned in close proximity to a calcium source (Dickman et al., 2008; Hoppa et al., 2012; Ly et al., 2008). Finally, it was recently shown that homeostasis occurs normally when *cac* levels are knocked down by 50% (Brusich et al., 2015). It is possible that homeostasis can still induce active zone reorganization and the upregulation of Cac levels despite this deficit.

Alternatively, another mechanism may compensate for decreased channel levels. Incorporating endogenously tagged channels into this experimental paradigm will enable a direct test of these alternatives.

How might active zone levels of calcium channels be regulated on a timescale of minutes? In agreement with an earlier study, we found that active zone cytomatrix levels of Brp also increase rapidly during homeostatic potentiation (Figure 6) (Weyhersmuller et al., 2011). Recent studies have found that active zone cytomatrix levels are also subject to rapid activity-dependent modification at mammalian cortical and hippocampal synapses (Cijsouw et al., 2014; Matz et al., 2010; Spangler et al., 2013). How does active zone reorganization translate into functional changes? Studies in both flies and mice have reported a link between the molecular content of the active zone cytomatrix and N (Bruckner et al., 2017; Matkovic et al., 2013; Matz et al., 2010; Reddy-Alla et al., 2017). We also observe a strong correlation between calcium channel and Brp levels at baseline and following homeostatic challenge, suggesting that reorganization of the active zone cytomatrix modulates the availability of sites for the incorporation of calcium channels to increase release probability (Figures 5,6) (Cao et al., 2004). This conclusion is consistent with loss-of-function phenotypes across phyla, which demonstrate both overall decreases in calcium channel clustering and impaired homeostatic potentiation in the absence of a number of active zone cytomatrix proteins (Bruckner et al., 2017; Frank et al., 2010; Graf et al., 2012; Kaeser et al., 2011; Kittel et al., 2006; Liu et al., 2011).

Weyhersmuller and colleagues assessed both N and P_v following the induction of presynaptic homeostatic potentiation and reorganization of the active zone cytomatrix, and found that N was significantly increased while P_v was increased to a lesser degree (Weyhersmuller et al., 2011). Increasing N while only modestly increasing, or even simply maintaining, P_v likely requires a concomitant increase in calcium channels to couple with newly recruited vesicles. Alternatively, calcium channels may influence N directly by constraining the number of vesicles that can dock in close enough proximity to a calcium source to be part of the readily releasable pool (Herman and Rosenmund, 2015). Notably, there is a growing body of evidence, to which this study adds, demonstrating that the interconnected parameters of calcium channel number, P_V, and N are strongly correlated with the size of the active zone, measured either by area in ultrastructural studies or the molecular content of the active zone cytomatrix in light-level studies (Cao et al., 2004; Ehmann et al., 2014; Holderith et al., 2012; Matz et al., 2010; Murthy et al., 2001; Peled and Isacoff, 2011; Propst and Ko, 1987; Reddy-Alla et al., 2017; Schikorski and Stevens, 1997). Taken together, these findings lead to the model that the active zone cytomatrix is a dynamic structure and conserved target for rapidly reorganizing synapses to support new release properties by simultaneously adding sites for calcium channels and release-ready vesicles (Figure 7).

A similar mechanism may underlie synaptic depression. A recent study of presynaptic long-term homeostatic depression at the *Drosophila* NMJ found that both the active zone cytomatrix and calcium channels are targeted for down-regulation (Gavino et al., 2015). In contrast, a study of light-induced synaptic remodeling in photoreceptors revealed downregulation of Brp, but no change in Cac levels (Sugie et al., 2015). As both studies employed overexpressed UAS-Cac-GFP, it will be interesting to determine if assessing endogenous channels changes either conclusion or if these observations reflect distinct mechanisms for modulating the active zone cytomatrix with and without altering calcium channel number.

While our experiments do not allow us to directly assess changes at single active zones, we found that the entire distribution of Brp and Cac levels shifted, as opposed to an increase in the percentage of high-Brp, high-Cac active zones within the established baseline range that would be expected if potentiation were achieved by converting silent or low-P_r active zones to high-P_r active zones. The generation of active zones with higher molecular content than observed at baseline is consistent with the previous observation that Brp levels appeared to be increased across all active zones during both short- and long-term homeostasis, and suggests that remodeling of active zones during homeostasis is not strictly limited to low-P_r active zones (Weyhersmuller et al., 2011). A recent functional analysis of single active zones during a 10-second, 5-Hz stimulus revealed functional changes at more than 85% of active zones (Newman et al., 2017). Surprisingly, these changes were diverse with both depression and facilitation observed within single motorneuron branches, again highlighting the important role single active zone analysis will play in advancing our understanding of how synaptic properties are regulated and our ability to accurately model neural circuits. Whether all of the active zone reorganization observed following presynaptic homeostatic potentiation translates into functional changes is not yet known. We cannot conclude that all of the observed increase in calcium channel clustering reflects membrane-inserted or active channels. In fact, a quantitative analysis suggests it may not. Following PhTx exposure, we observe an average increase of ~50% in total active zone Cac levels. This translates into an ~40% increase in quantal content, which is smaller than predicted by the nonlinear relationship between calcium concentration and neurotransmitter release (Dodge and Rahamimoff, 1967; Jan and Jan, 1976) (Figure 6 and Figure 6—figure supplement 1).

The generation of engineered lines that enable the specific monitoring membrane-inserted calcium channels will facilitate a direct examination of this question.

Future studies that directly monitor how functionally distinct active zones participate in the modulation of P_r during acute homeostasis will also be of interest. These experiments are technically challenging; because acute presynaptic homeostatic potentiation is highly vulnerable to any stretching of postsynaptic muscles, PhTx is applied to partially dissected preparations that are inaccessible to imaging. Reliably overcoming this obstacle will yield an excellent model for following individual active zones of known molecular and functional states as they respond to homeostatic challenge, as will the investigation of the molecular changes that underlie other forms of short-term plasticity at single active zones. Endogenous tagging of Cac provides a valuable reagent for understanding how the distribution of calcium channels and their relationship to synaptic vesicles defines distinct presynaptic release properties and how their reorganization contributes to synaptic plasticity.

Materials and methods

Drosophila genetics and genome engineering

The following fly lines are available at the Bloomington *Drosophila* Stock Center (BDSC): w^{1118} (BDSC #5905), *vasa-Cas9* (BDSC #51324), and piggyBac transposase lines (BDSC #8285, #32070 or #32073) (Gratz et al., 2014; Horn et al., 2003; Parks et al., 2004). PS-GCaMP comprises an MHC promoter for muscle expression, an N-terminal myristoylation sequence for membrane targeting, GCaMP5, and the Shaker PDZ domain for targeting to the postsynaptic density, and was incorporated into the attP2 landing site (BDSC-25710). Endogenously tagged Cacophony was generated using a scarless CRISPR/piggyBac-based approach (flyCRISPR.molbio.wisc.edu). Briefly, sequences coding for sfGFP or TagRFP-T flanked by flexible linkers and a visible marker flanked by piggyBac inverted terminal repeat sequences were inserted immediately downstream of the transcriptional start site of the endogenous *Cacophony* locus (basepairs 11,980,057 through 11,980,055, *D. melanogaster* genome release 6). This site is in an exon common to all isoforms of *Cac*. piggyBac transposase was subsequently used for footprint-free removal of the marker, followed by molecular confirmation of precise tag incorporation.

Calcium imaging and analysis

Calcium influx at motor terminals was measured by forward filling of dextran-conjugated indicators (Macleod, 2012). Third instar larva were dissected in chilled Schneider's insect medium (Sigma). Severed segmental nerves were drawn into a filling pipette, and a 16:1 mixture of the calcium indicator rhod dextran (R34676; Thermo Fisher Scientific) and a calcium-insensitive Alexa Fluor 647 dextran (AF647 dextran; D22914; Thermo Fisher Scientific) was applied to the cut nerve end for 15-45 minutes. Preparations were incubated in the dark for at least 3 hours and rinsed every 30 minutes with fresh Schneider's insect medium. Thirty minutes before imaging, the Schneider's insect medium was replaced with hemolymph-like solution (HL6) containing 2.0 mM Ca^{2+} and supplemented with 7 mM L-glutamic acid (Macleod et al., 2002). Analysis was performed on type-Ib and type-Is motor neuron terminals innervating muscle 6 in hemisegment A2 or A3. Live imaging was performed on a Nikon Eclipse FN1 microscope with a 100x 1.1NA water immersion objective (Nikon) using an iXon3 888 EMCCD camera (Andor) operating at a frame rate of 114 Hz. The terminals were alternately excited at 550 ± 7nm and 640 ± 15nm, and emission was alternately collected at 605 ± 26nm and 705 ± 36nm, respectively. The cut end of the segmental nerve was stimulated using a 0.4-ms pulse 10 times at 1 Hz followed by a stimulus train at 20 Hz for one second. Images were processed with NIS-Elements Ar (Nikon). Following background subtraction, florescence intensity traces were generated for an ROI encompassing two or more non-terminal boutons. Ca^{2+} levels are measured as the fluorescence ratio of rhod to AF647. Ten single action potentials were averaged into a single trace and used to calculate peak amplitude and the decay time constant (tau).

Electrophysiology

Male third instar larvae were dissected in Ca^{2+}-free hemolymph-like saline (HL3, 70 mM NaCl, 5 mM KCl, 20 mM MgCl2, 10 mM NaHCO3, 115 mM sucrose, 5 mM trehalose, 5 mM HEPES, pH 7.2) (Stewart et al., 1994). Recordings were performed in HL3 saline containing 0.6 mM Ca^{2+}. For current clamp recordings, a sharp borosilicate electrode (resistance of 15-25 MΩ) filled with 3M KCl was used to record from muscle 6 of segments A3 and A4. All dissections and recordings were performed at 25°C, and all cells analyzed had an initial resting potential between -60 and -80 mV and input resistance ≥ 5 MΩ. For each cell, 60 consecutive mEJPs were collected with pClamp (Molecular Devices) and analyzed using MiniAnalysis (Synaptosoft) to obtain mean amplitude. EJPs were stimulated by applying a 1-ms pulse to the cut end of the segmental nerve innervating the impaled muscle cell. Stimulus amplitude was adjusted to reliably recruit both the Ib and Is inputs onto muscle 6, and at least 30 consecutive EJPs were recorded for each cell, analyzed in pClamp to obtain mean amplitude, and corrected for nonlinear summation (McLachlan and Martin, 1981). Quantal content was calculated for each NMJ as mean corrected EJP amplitude divided by mean mEJP amplitude.

Pharmacological homeostatic challenge was assessed by incubating semi-intact preparations in 20 μM Philanthotoxin-433 (Santa Cruz) diluted in HL3 containing 2.0 mM Ca^{2+} for 10 min at 25 degrees (Frank et al., 2006). Following treatment, the dissection was completed and the prep was rinsed 5 times in recording solution. During the dissection, care was taken to avoid stretching of body wall muscles, which blocks the induction of homeostasis (Frank et al., 2006).

Immunostaining

Male third instar larvae were dissected in ice-cold Ca^{2+}-free saline and fixed for 30 minutes in 4% paraformaldehyde in PBS. Dissected larvae were washed and permeabilized in PBS containing 0.1% Triton-X and blocked overnight at 4°C in PBS containing 0.1% Triton-X and 1% BSA. Dissected larvae were incubated in primary antibodies overnight at 4°C or 3 hours at room temperature and secondary antibodies for 2 hours at room temperature, then mounted in Vectashield (Vector Laboratories) or ProLong Diamond (ThermoFisher). For immunostaining experiments following homeostatic challenge, preparations were treated as described for electrophysiological experiments, fixed with 4% PFA for 30 minutes, and stained as above. The following antibodies were used at the indicated concentrations: mouse anti-Brp at 1:100 (Nc82; developed by Erich Buchner and obtained from the Developmental Studies Hybridoma Bank), rabbit anti-GFP conjugated to AlexaFluor 488 at 1:500 (#A21311, ThermoFisher), and anti-HRP conjugated to AlexaFluor 647 at 1:500 (Jackson ImmunoResearch). Species-specific Alexa Fluor 488 and 568 secondary antibodies (Invitrogen) were used at 1:500.

Confocal imaging and analysis

Confocal images were acquired on a Nikon A1R-Si+ with Plan-Apo 60x (1.40 NA) oil immersion objective (UW-Madison Biochemistry Optical Core) or Olympus Fluoview FV1000 with Plan-Apo 60x (1.42 NA) oil immersion objective. Image analyses and brightness and contrast adjustments were performed using the Fiji distribution of ImageJ (Schindelin et al., 2012). For analysis of Cac and Brp intensity, all genotypes were stained together and imaged with identical settings. For consistency, analysis was limited to NMJ 6/7 in segments A2 and A3. To measure $Cac^{sfGFP-N}$ and Brp intensity at individual active zones, nonsynaptic structures including axons were removed from the images using freehand selection and fill. Z-stacks were flattened using the Maximum Intensity Z-projection function. Channels were separated, background subtracted, and noise was reduced using a light Gaussian filter (0.75-pixel sigma radius). A threshold was applied to the Brp channel to remove irrelevant low intensity pixels and individual puncta were identified and segmented using the Find Maxima tool. The resulting segmented Brp image was used to create a binary mask that was also used to segment the $Cac^{sfGFP-N}$ channel. Intensity data were collected using the Analyze Particles tool. Total intensity per active zone is calculated as the product of average intensity and particle area.

Functional imaging

Functional imaging experiments were performed using a Nikon A1R+ scanning confocal system built on a Nikon Eclipse FN1 microscope with a CFI Plan 100XW objective (Nikon). $Cac^{TagRFP-N}$; PS-GCaMP third instar male larvae were dissected in ice-cold Ca^{2+}-free HL3 and severed segmental nerves were drawn into a stimulating pipette. Preparations were then maintained in HL3 saline containing 1.5 mM Ca^{2+} and 25 mM Mg^{2+} for imaging. Type-Ib motor neuron terminals innervating muscle 6 in hemisegment A2 or A3 were first imaged using the galvanometer scanner to collect a $Cac^{TagRFP-N}$ Z-stack. GCaMP5 was then imaged continuously in a single focal plane using the resonant scanner with full frame averaging for a final acquisition rate of 15.3 frames per second. Evoked postsynaptic calcium transients were stimulated by applying a 0.4-ms pulse every second. The stimulus amplitude was adjusted to reliably recruit the Ib input. 94-100 stimulations were recorded for each experiment. $Cac^{TagRFP-N}$ was analyzed in Fiji. Z-stacks were flattened using the Maximum Intensity Z-projection function. To identify individual $Cac^{TagRFP-N}$ puncta, a mask was created using a gaussian filter (sigma radius = 2) and unsharp mask (radius = 3, weight = 0.8). A threshold was then applied to the mask to remove lower intensity pixels between puncta and individual puncta were segmented using the Find Maxima tool. By identifying large puncta with two local intensity maxima, the Find Maxima tool facilitates the identification and segmentation of closely spaced active zones. From the resulting image, we created a binary mask that was used to isolate puncta in the original Z-projection. Each punctum was then interrogated for intensity and XY coordinates using the Analyze Particles tool. GCaMP movies were processed using Nikon Elements software. Motion artifacts during acquisition were corrected by aligning all frames to the first frame of the movie. Baseline fluorescence was subtracted from every frame using a frame created from the average of 10 non-stimulus frames that also lacked spontaneous release events, and noise was reduced using the Nikon Elements Advanced Denoising function. The XY coordinates of postsynaptic calcium transients were collected from all stimulation frames manually or automatically. For manual analysis, XY coordinates were obtained using hand selection of individual fluorescence peaks. Only peaks that persisted and decayed over subsequent frames were recorded. For automated analysis, all stimulation frames were thresholded to remove background noise and the Find Maxima tool in Fiji was used to identify event XY coordinates. Each postsynaptic event was then assigned to a $Cac^{TagRFP-N}$

punctum through nearest neighbor analysis using euclidean distance.

Statistical analyses
Statistical analyses were conducted in GraphPad Prism 7. Single comparisons of normally distributed datasets, as determined by the D'Agostino-Pearson omnibus test, were conducted by Student's t test. Welch's correction was used in cases of unequal variance. The Mann-Whitney U test was used for single comparisons of non-normally distributed data. Kruskal-Wallis tests were used to compare pooled frequency distributions for different conditions. One-dimensional Pearson correlation coefficients (r) were used to compare intensity levels and release probability. Reported values are mean ± SEM unless otherwise stated. P values and sample sizes are reported in each figure legend.

Acknowledgements
The Developmental Studies Hybridoma Bank and the Bloomington *Drosophila* Stock Center provided antibodies and fly stocks. We are grateful to Fiona Ukken for generating postsynaptically targeted GCaMP5 and Hong Zhan for assistance with data analysis and visualization. We thank Elle Kielar-Grevstad, Director of the UW-Madison Biochemistry Optical Core, for assistance with image analysis and Sean Carroll for generously sharing equipment. We thank Andy Frank, Dion Dickman, and Pragya Goel for insightful discussions and members of the Macleod and O'Connor-Giles labs for critical comments on the work. This work was supported by grants from the National Institute of Neurological Disorders and Stroke, National Institutes of Health to K.M.O.G (R01NS078179 and R21NS088830) and G.T.M. (R01NS061914) and a McKnight Technological Innovations in Neuroscience Award to K.M.O.G.

References
Ackermann, F., C.L. Waites, and C.C. Garner. 2015. Presynaptic active zones in invertebrates and vertebrates. *EMBO reports*. 16:923-938.

Atwood, H.L., and S. Karunanithi. 2002. Diversification of synaptic strength: presynaptic elements. *Nature reviews. Neuroscience*. 3:497-516.

Bohme, M.A., C. Beis, S. Reddy-Alla, E. Reynolds, M.M. Mampell, A.T. Grasskamp, J. Lutzkendorf, D.D. Bergeron, J.H. Driller, H. Babikir, F. Gottfert, I.M. Robinson, C.J. O'Kane, S.W. Hell, M.C. Wahl, U. Stelzl, B. Loll, A.M. Walter, and S.J. Sigrist. 2016. Active zone scaffolds differentially accumulate Unc13 isoforms to tune Ca(2+) channel-vesicle coupling. *Nature neuroscience*. 19:1311-1320.

Branco, T., and K. Staras. 2009. The probability of neurotransmitter release: variability and feedback control at single synapses. *Nature reviews. Neuroscience*. 10:373-383.

Brenowitz, S.D., and W.G. Regehr. 2007. Reliability and heterogeneity of calcium signaling at single presynaptic boutons of cerebellar granule cells. *The Journal of neuroscience : the official journal of the Society for Neuroscience*. 27:7888-7898.

Bruckner, J.J., S.J. Gratz, J.K. Slind, R.R. Geske, A.M. Cummings, S.E. Galindo, L.K. Donohue, and K.M. O'Connor-Giles. 2012. Fife, a Drosophila Piccolo-RIM homolog, promotes active zone organization and neurotransmitter release. *The Journal of neuroscience : the official journal of the Society for Neuroscience*. 32:17048-17058.

Bruckner, J.J., H. Zhan, S.J. Gratz, M. Rao, F. Ukken, G. Zilberg, and K.M. O'Connor-Giles. 2017. Fife organizes synaptic vesicles and calcium channels for high-probability neurotransmitter release. *The Journal of cell biology*. 216:231-246.

Brusich, D.J., A.M. Spring, and C.A. Frank. 2015. A single-cross, RNA interference-based genetic tool for examining the long-term maintenance of homeostatic plasticity. *Frontiers in cellular neuroscience*. 9:107.

Cao, Y.Q., E.S. Piedras-Renteria, G.B. Smith, G. Chen, N.C. Harata, and R.W. Tsien. 2004. Presynaptic Ca2+ channels compete for channel type-preferring slots in altered neurotransmission arising from Ca2+ channelopathy. *Neuron*. 43:387-400.

Cijsouw, T., J.P. Weber, J.H. Broeke, J.A. Broek, D. Schut, T. Kroon, I. Saarloos, M. Verhage, and R.F. Toonen. 2014. Munc18-1 redistributes in nerve terminals in an activity- and PKC-dependent manner. *The Journal of cell biology*. 204:759-775.

Cull-Candy, S.G., R. Miledi, A. Trautmann, and O.D. Uchitel. 1980. On the release of transmitter at normal, myasthenia gravis and myasthenic syndrome affected human end-plates. *The Journal of physiology*. 299:621-638.

Davis, G.W., and M. Muller. 2015. Homeostatic control of presynaptic neurotransmitter release. *Annual review of physiology*. 77:251-270.

Del Castillo, J., and B. Katz. 1954. Quantal components of the end-plate potential. *The Journal of physiology*. 124:560-573.

Dickman, D.K., P.T. Kurshan, and T.L. Schwarz. 2008. Mutations in a Drosophila alpha2delta voltage-gated calcium channel subunit reveal a crucial synaptic function. *The Journal of neuroscience : the official journal of the Society for Neuroscience*. 28:31-38.

Dodge, F.A., Jr., and R. Rahamimoff. 1967. Co-operative action a calcium ions in transmitter release at the neuromuscular junction. *The Journal of physiology*. 193:419-432.

Ehmann, N., S. van de Linde, A. Alon, D. Ljaschenko, X.Z. Keung, T. Holm, A. Rings, A. DiAntonio, S. Hallermann, U. Ashery, M. Heckmann, M. Sauer, and R.J. Kittel. 2014. Quantitative super-resolution imaging of Bruchpilot distinguishes active zone states. *Nature communications*. 5:4650.

Ermolyuk, Y.S., F.G. Alder, C. Henneberger, D.A. Rusakov, D.M. Kullmann, and K.E. Volynski. 2012. Independent regulation of basal neurotransmitter release efficacy by variable Ca(2)+ influx and bouton size at small central synapses. *PLoS biology*. 10:e1001396.

Frank, C.A. 2014. Homeostatic plasticity at the Drosophila neuromuscular junction. *Neuropharmacology*. 78:63-74.

Frank, C.A., M.J. Kennedy, C.P. Goold, K.W. Marek, and G.W. Davis. 2006. Mechanisms underlying the rapid induction and sustained expression of synaptic homeostasis. *Neuron*. 52:663-677.

Frank, T., M.A. Rutherford, N. Strenzke, A. Neef, T. Pangrsic, D. Khimich, A. Fejtova, E.D. Gundelfinger, M.C. Liberman, B. Harke, K.E. Bryan, A. Lee, A. Egner, D. Riedel, and T. Moser. 2010. Bassoon and the synaptic ribbon organize Ca(2)+ channels and vesicles to add release sites and promote refilling. *Neuron*. 68:724-738.

Gavino, M.A., K.J. Ford, S. Archila, and G.W. Davis. 2015. Homeostatic synaptic depression is achieved through a regulated decrease in presynaptic calcium channel abundance. *eLife*. 4.

Graf, E.R., R.W. Daniels, R.W. Burgess, T.L. Schwarz, and A. DiAntonio. 2009. Rab3 dynamically controls protein composition at active zones. *Neuron*. 64:663-677.

Graf, E.R., V. Valakh, C.M. Wright, C. Wu, Z. Liu, Y.Q. Zhang, and A. DiAntonio. 2012. RIM promotes calcium channel accumulation at active zones of the Drosophila neuromuscular junction. *The Journal of neuroscience : the official journal of the Society for Neuroscience*. 32:16586-16596.

Gratz, S.J., F.P. Ukken, C.D. Rubinstein, G. Thiede, L.K. Donohue, A.M. Cummings, and K.M. O'Connor-Giles. 2014. Highly specific and efficient CRISPR/Cas9-catalyzed homology-directed repair in Drosophila. *Genetics*. 196:961-971.

Guerrero, G., D.F. Reiff, G. Agarwal, R.W. Ball, A. Borst, C.S. Goodman, and E.Y. Isacoff. 2005. Heterogeneity in synaptic transmission along a Drosophila larval motor axon. *Nature neuroscience*. 8:1188-1196.

Harris, K.P., and J.T. Littleton. 2015. Transmission, Development, and Plasticity of Synapses. *Genetics*. 201:345-375.

Hatt, H., and D.O. Smith. 1976. Non-uniform probabilities of quantal release at the crayfish neuromuscular junction. *The Journal of physiology*. 259:395-404.

Herman, M.A., and C. Rosenmund. 2015. On the brink: a new synaptic vesicle release model at the calyx of held. *Neuron*. 85:6-8.

Holderith, N., A. Lorincz, G. Katona, B. Rozsa, A. Kulik, M. Watanabe, and Z. Nusser. 2012. Release probability of hippocampal glutamatergic terminals scales with the size of the active zone. *Nature neuroscience*. 15:988-997.

Homan, A.E., R. Laghaei, M. Dittrich, and S.D. Meriney. 2017. The impact of spatio-temporal calcium dynamics within presynaptic active zones on synaptic delay at the frog neuromuscular junction. *Journal of neurophysiology*:jn 00510 02017.

Hoppa, M.B., B. Lana, W. Margas, A.C. Dolphin, and T.A. Ryan. 2012. alpha2delta expression sets presynaptic calcium channel abundance and release probability. *Nature*. 486:122-125.

Horn, C., N. Offen, S. Nystedt, U. Hacker, and E.A. Wimmer. 2003. piggyBac-based insertional mutagenesis and enhancer detection as a tool for functional insect genomics. *Genetics*. 163:647-661.

Indriati, D.W., N. Kamasawa, K. Matsui, A.L. Meredith, M. Watanabe, and R. Shigemoto. 2013. Quantitative localization of Cav2.1 (P/Q-type) voltage-dependent calcium channels in Purkinje cells: somatodendritic gradient and distinct somatic coclustering with calcium-activated potassium channels. *The Journal of neuroscience : the official journal of the Society for Neuroscience*. 33:3668-3678.

Jan, L.Y., and Y.N. Jan. 1976. Properties of the larval neuromuscular junction in Drosophila melanogaster. *The Journal of physiology*. 262:189-214.

Kaeser, P.S., L. Deng, Y. Wang, I. Dulubova, X. Liu, J. Rizo, and T.C. Sudhof. 2011. RIM proteins tether Ca2+ channels to presynaptic active zones via a direct PDZ-domain interaction. *Cell*. 144:282-295.

Kawasaki, F., S.C. Collins, and R.W. Ordway. 2002. Synaptic calcium-channel function in Drosophila: analysis and transformation rescue of temperature-sensitive paralytic and lethal mutations of cacophony. *The Journal of neuroscience : the official journal of the Society for Neuroscience*. 22:5856-5864.

Kawasaki, F., B. Zou, X. Xu, and R.W. Ordway. 2004. Active zone localization of presynaptic calcium channels encoded by the cacophony locus of Drosophila. *The Journal of neuroscience : the official journal of the Society for Neuroscience*. 24:282-285.

Keller, D., N. Babai, O. Kochubey, Y. Han, H. Markram, F. Schurmann, and R. Schneggenburger. 2015. An Exclusion Zone for Ca2+ Channels around Docked Vesicles Explains Release Control by Multiple Channels at a CNS Synapse. *PLoS computational biology*. 11:e1004253.

Kittel, R.J., C. Wichmann, T.M. Rasse, W. Fouquet, M. Schmidt, A. Schmid, D.A. Wagh, C. Pawlu, R.R. Kellner, K.I. Willig, S.W. Hell, E. Buchner, M. Heckmann, and S.J. Sigrist. 2006. Bruchpilot promotes active zone assembly, Ca2+ channel clustering, and vesicle release. *Science*. 312:1051-1054.

Liu, K.S., M. Siebert, S. Mertel, E. Knoche, S. Wegener, C. Wichmann, T. Matkovic, K. Muhammad, H. Depner, C. Mettke, J. Buckers, S.W. Hell, M. Muller, G.W. Davis, D. Schmitz, and S.J. Sigrist. 2011. RIM-binding protein, a central part of the active zone, is essential for neurotransmitter release. *Science*. 334:1565-1569.

Lu, Z., A.K. Chouhan, J.A. Borycz, Z. Lu, A.J. Rossano, K.L. Brain, Y. Zhou, I.A. Meinertzhagen, and G.T. Macleod. 2016. High-Probability Neurotransmitter Release Sites Represent an Energy-Efficient Design. *Current biology : CB*. 26:2562-2571.

Ly, C.V., C.K. Yao, P. Verstreken, T. Ohyama, and H.J. Bellen. 2008. straightjacket is required for the synaptic stabilization of cacophony, a voltage-gated calcium channel alpha1 subunit. *The Journal of cell biology*. 181:157-170.

Macleod, G.T. 2012. Forward-filling of dextran-conjugated indicators for calcium imaging at the Drosophila larval neuromuscular junction. *Cold Spring Harbor protocols*. 2012:791-796.

Macleod, G.T., M. Hegstrom-Wojtowicz, M.P. Charlton, and H.L. Atwood. 2002. Fast calcium signals in Drosophila motor neuron terminals. *Journal of neurophysiology*. 88:2659-2663.

Matkovic, T., M. Siebert, E. Knoche, H. Depner, S. Mertel, D. Owald, M. Schmidt, U. Thomas, A. Sickmann, D. Kamin, S.W. Hell, J. Burger, C. Hollmann, T. Mielke, C. Wichmann, and S.J. Sigrist. 2013. The Bruchpilot cytomatrix determines the size of the readily releasable pool of synaptic vesicles. *The Journal of cell biology*. 202:667-683.

Matz, J., A. Gilyan, A. Kolar, T. McCarvill, and S.R. Krueger. 2010. Rapid structural alterations of the active zone lead to sustained changes in neurotransmitter release. *Proceedings of the National Academy of Sciences of the United States of America*. 107:8836-8841.

McLachlan, E.M., and A.R. Martin. 1981. Non-linear summation of end-plate potentials in the frog and mouse. *The Journal of physiology*. 311:307-324.

Meinrenken, C.J., J.G. Borst, and B. Sakmann. 2002. Calcium secretion coupling at calyx of Held governed by nonuniform channel-vesicle topography. *The Journal of neuroscience : the official journal of the Society for Neuroscience*. 22:1648-1667.

Melom, J.E., Y. Akbergenova, J.P. Gavornik, and J.T. Littleton. 2013. Spontaneous and evoked release are independently regulated at individual active zones. *The Journal of neuroscience : the official journal of the Society for Neuroscience*. 33:17253-17263.

Muller, M., O. Genc, and G.W. Davis. 2015. RIM-binding protein links synaptic homeostasis to the stabilization and replenishment of high release probability vesicles. *Neuron*. 85:1056-1069.

Muller, M., K.S. Liu, S.J. Sigrist, and G.W. Davis. 2012. RIM controls homeostatic plasticity through modulation of the readily-releasable vesicle pool. *The Journal of neuroscience : the official journal of the Society for Neuroscience*. 32:16574-16585.

Murthy, V.N., T. Schikorski, C.F. Stevens, and Y. Zhu. 2001. Inactivity produces increases in neurotransmitter release and synapse size. *Neuron*. 32:673-682.

Nakamura, Y., H. Harada, N. Kamasawa, K. Matsui, J.S. Rothman, R. Shigemoto, R.A. Silver, D.A. DiGregorio, and T. Takahashi. 2015. Nanoscale distribution of presynaptic Ca(2+) channels and its impact on vesicular release during development. *Neuron*. 85:145-158.

Newman, Z.L., A. Hoagland, K. Aghi, K. Worden, S.L. Levy, J.H. Son, L.P. Lee, and E.Y. Isacoff. 2017. Input-Specific Plasticity and Homeostasis at the Drosophila Larval Neuromuscular Junction. *Neuron*. 93:1388-1404 e1310.

Owald, D., W. Fouquet, M. Schmidt, C. Wichmann, S. Mertel, H. Depner, F. Christiansen, C. Zube, C. Quentin, J. Korner, H. Urlaub, K. Mechtler, and S.J. Sigrist. 2010. A Syd-1 homologue regulates pre- and postsynaptic maturation in Drosophila. *The Journal of cell biology*. 188:565-579.

Parks, A.L., K.R. Cook, M. Belvin, N.A. Dompe, R. Fawcett, K. Huppert, L.R. Tan, C.G. Winter, K.P. Bogart, J.E. Deal, M.E. Deal-Herr, D. Grant, M. Marcinko, W.Y. Miyazaki, S. Robertson, K.J. Shaw, M. Tabios, V. Vysotskaia, L. Zhao, R.S. Andrade, K.A. Edgar, E. Howie, K. Killpack, B. Milash, A. Norton, D. Thao, K. Whittaker, M.A. Winner, L. Friedman, J. Margolis, M.A. Singer, C. Kopczynski, D. Curtis, T.C. Kaufman, G.D. Plowman, G. Duyk, and H.L. Francis-Lang. 2004. Systematic generation of high-resolution deletion coverage of the Drosophila melanogaster genome. *Nature genetics*. 36:288-292.

Pawson, P.A., and A.D. Grinnell. 1984. Posttetanic potentiation in strong and weak neuromuscular junctions: physiological differences caused by a differential Ca2+-influx. *Brain research*. 323:311-315.

Peled, E.S., and E.Y. Isacoff. 2011. Optical quantal analysis of synaptic transmission in wild-type and rab3-mutant Drosophila motor axons. *Nature neuroscience*. 14:519-526.

Peled, E.S., Z.L. Newman, and E.Y. Isacoff. 2014. Evoked and spontaneous transmission favored by distinct sets of synapses. *Current biology : CB*. 24:484-493.

Petzoldt, A.G., J. Lutzkendorf, and S.J. Sigrist. 2016. Mechanisms controlling assembly and plasticity of presynaptic active zone scaffolds. *Current opinion in neurobiology*. 39:69-76.

Propst, J.W., and C.P. Ko. 1987. Correlations between active zone ultrastructure and synaptic function studied with freeze-fracture of physiologically identified neuromuscular junctions. *The Journal of neuroscience : the official journal of the Society for Neuroscience*. 7:3654-3664.

Reddy-Alla, S., M.A. Bohme, E. Reynolds, C. Beis, A.T. Grasskamp, M.M. Mampell, M. Maglione, M. Jusyte, U. Rey, H. Babikir, A.W. McCarthy, C. Quentin, T. Matkovic, D.D. Bergeron, Z. Mushtaq, F. Gottfert, D. Owald, T. Mielke, S.W. Hell, S.J. Sigrist, and A.M. Walter. 2017. Stable Positioning of Unc13 Restricts Synaptic Vesicle Fusion to Defined Release Sites to Promote Synchronous Neurotransmission. *Neuron*. 95:1350-1364 e1312.

Rieckhof, G.E., M. Yoshihara, Z. Guan, and J.T. Littleton. 2003. Presynaptic N-type calcium channels regulate synaptic growth. *The Journal of biological chemistry*. 278:41099-41108.

Schikorski, T., and C.F. Stevens. 1997. Quantitative ultrastructural analysis of hippocampal excitatory synapses. *The Journal of neuroscience : the official journal of the Society for Neuroscience*. 17:5858-5867.

Sheng, J., L. He, H. Zheng, L. Xue, F. Luo, W. Shin, T. Sun, T. Kuner, D.T. Yue, and L.G. Wu. 2012. Calcium-channel number critically influences synaptic strength and plasticity at the active zone. *Nature neuroscience*. 15:998-1006.

Spangler, S.A., S.K. Schmitz, J.T. Kevenaar, E. de Graaff, H. de Wit, J. Demmers, R.F. Toonen, and C.C. Hoogenraad. 2013. Liprin-alpha2 promotes the presynaptic recruitment and turnover of RIM1/CASK to facilitate synaptic transmission. *The Journal of cell biology*. 201:915-928.

Stewart, B.A., H.L. Atwood, J.J. Renger, J. Wang, and C.F. Wu. 1994. Improved stability of Drosophila larval neuromuscular preparations in haemolymph-like physiological solutions. *Journal of comparative physiology. A, Sensory, neural, and behavioral physiology*. 175:179-191.

Sugie, A., S. Hakeda-Suzuki, E. Suzuki, M. Silies, M. Shimozono, C. Mohl, T. Suzuki, and G. Tavosanis. 2015. Molecular Remodeling of the Presynaptic Active Zone of Drosophila Photoreceptors via Activity-Dependent Feedback. *Neuron*. 86:711-725.

Wang, T., R.T. Jones, J.M. Whippen, and G.W. Davis. 2016. alpha2delta-3 Is Required for Rapid Transsynaptic Homeostatic Signaling. *Cell reports*. 16:2875-2888.

Weyhersmuller, A., S. Hallermann, N. Wagner, and J. Eilers. 2011. Rapid active zone remodeling during synaptic plasticity. *The Journal of neuroscience : the official journal of the Society for Neuroscience*. 31:6041-6052.

Xu-Friedman, M.A., K.M. Harris, and W.G. Regehr. 2001. Three-dimensional comparison of ultrastructural characteristics at depressing and facilitating synapses onto cerebellar Purkinje cells. *The Journal of neuroscience : the official journal of the Society for Neuroscience*. 21:6666-6672.

Younger, M.A., M. Muller, A. Tong, E.C. Pym, and G.W. Davis. 2013. A presynaptic ENaC channel drives homeostatic plasticity. *Neuron*. 79:1183-1196.

Zhan, H., J. Bruckner, Z. Zhang, and K. O'Connor-Giles. 2016. Three-dimensional imaging of Drosophila motor synapses reveals ultrastructural organizational patterns. *Journal of neurogenetics*. 30:237-246.

Figure 1

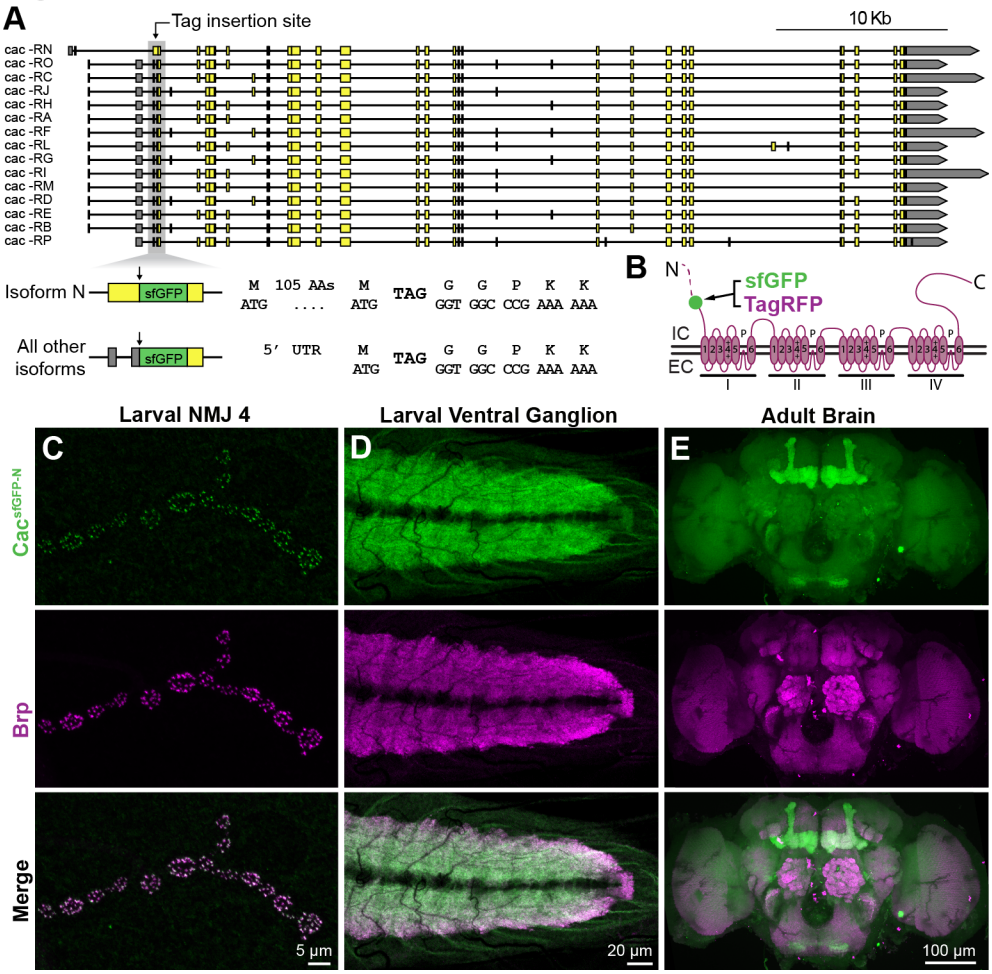

Figure 1. Endogenously tagged Cacophony calcium channels localize to synapses. (**A**) *cacophony* locus indicating the site of tag incorporation in all isoforms. The tag is incorporated between amino acids 107 and 108 of isoform N and immediately following the start methionine in all other isoforms. (**B**) Schematic of endogenously tagged Cacophony protein indicating the site of tag incorporation (green dot). The longer N-terminus of isoform N is represented by a dotted line. EC – extracellular, IC – intracellular. (**C-E**) Confocal Z-projection of a *cac*$^{sfGFP\text{-}N}$ larval NMJ (**C**), larval ventral ganglion (**D**), and adult brain (**E**) co-labeled with antibodies against GFP and Brp.

Figure 2

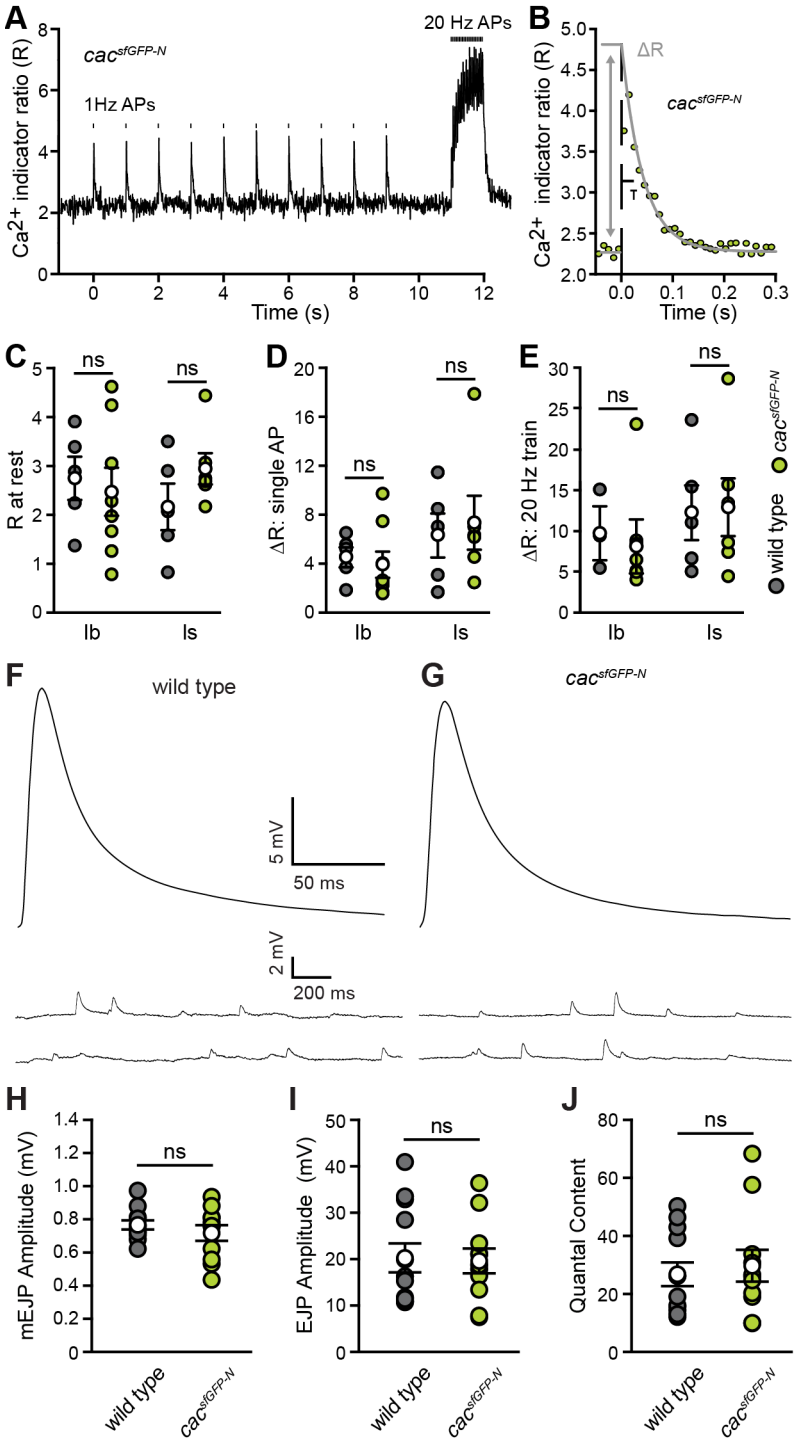

Figure 2. Endogenously tagged Cacophony calcium channels exhibit normal calcium influx and support normal neurotransmitter release. (**A**) Traces of the fluorescence changes in rhod-dextran (relative to AF647-dextran) in response to 10 action potentials initiated at the times indicated. An action potential is initiated every second, followed by a 1-sec, 20-Hz train of action potentials. (**B**) Plot of the average of 10 fluorescence responses to single action potentials. The amplitude of single action potential-mediated Ca^{2+} transients was determined by projecting the decay phase back to the time of the stimulus and subtracting R at this time from the baseline immediately

before the stimulus. (**C**) Plot of the average Ca^{2+} levels (R) in terminals prior to nerve stimulation for type-Ib and -Is terminals in *cac*$^{sfGFP-N}$ and wild-type larvae (wild type Ib, 2.74 ± 0.44, n=5 NMJs; *cac*$^{sfGFP-N}$ Ib, 2.47 ± 0.49, n=8 NMJs, p=0.69; wild type Is, 2.16 ± 0.47, n=5 NMJs; *cac*$^{sfGFP-N}$ Is, 2.94 ± 0.32, n=6 NMJs, p=0.21; Student's t test). (**D**) Plot of the average amplitude of single action potential-mediated Ca^{2+} transients (ΔR) (wild-type Ib, 4.50 ± 0.81, n=5 NMJs; *cac*$^{sfGFP-N}$ Ib, 3.90 ± 1.07, n=8 NMJs, p=0.67; wild-type Is, 6.28 ± 1.79, n=5 NMJs; *cac*$^{sfGFP-N}$ Is, 7.33 ± 2.20, n=6 NMJs, p=0.72; Student's t test). (**E**) Plot of the average amplitude of 1-sec, 20-Hz AP train-mediated Ca^{2+} transients (wild-type Ib, 9.71 ± 1.53, n=5 NMJs; *cac*$^{sfGFP-N}$ Ib, 8.13 ± 2.21, n=8 NMJs, p=0.57; wild-type Is, 12.26 ± 3.36, n=5 NMJs; *cac*$^{sfGFP-N}$ Is, 12.94 ± 3.45, n=6 NMJs, p=0.89; Student's t test). (**F-G**) Representative traces of EJPs and mEJPs recorded in 0.6 mM Ca^{2+} at wild-type (**F**) and *cac*$^{sfGFP-N}$ (**G**) NMJs. Stimulus artifacts have been removed for clarity. (**H**) mEJP amplitude is unaffected *cac*$^{sfGFP-N}$ (wild type, 0.77 ± 0.03, n=12 NMJs from 4 larvae; *cac*$^{sfGFP-N}$, 0.72 ± 0.05, n=11 NMJs from 7 larvae, p=0.37). (**I**) EJP amplitude is unchanged between wild-type and *cac*$^{sfGFP-N}$ NMJs (wild type, 20.28 ± 3.12, n=12 NMJs from 4 larvae; *cac*$^{sfGFP-N}$, 19.64 ± 2.69, n=11 NMJs from 7 larvae, p=0.88). (**J**) Quantal content is similar between wild-type and *cac*$^{sfGFP-N}$ NMJs (wild type, 26.8 ± 4.1, n=12 NMJs from 4 larvae; *cac*$^{sfGFP-N}$, 29.7 ± 5.5, n=11 NMJs from 7 larvae, p=0.67).

Figure 3

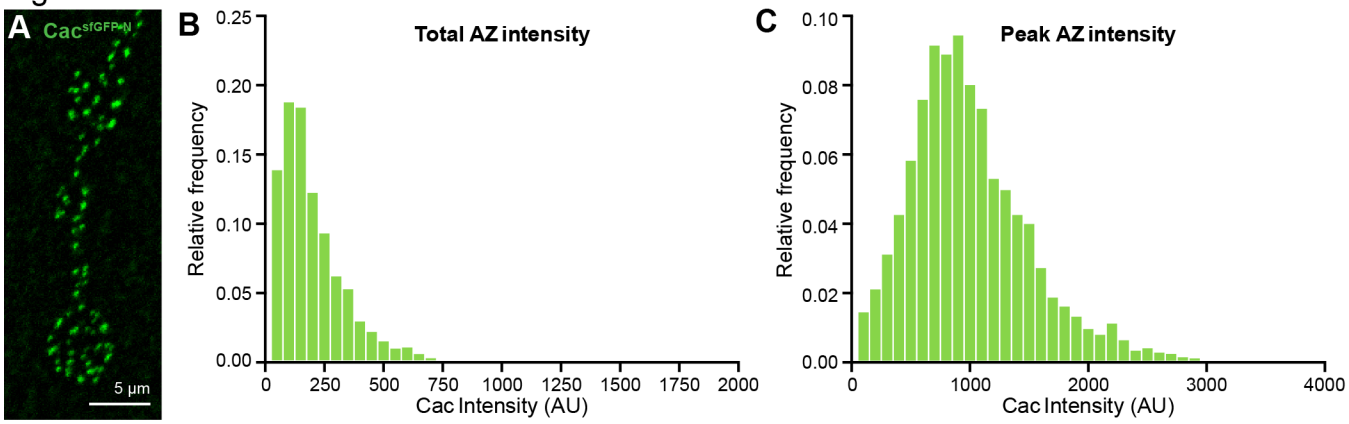

Figure 3. Cac$^{sfGFP-N}$ is differentially localized at individual active zones of single motorneurons. (**A**) Confocal Z-projection of a *cac$^{sfGFP-N}$* larval NMJ labeled with an antibody against GFP. (**B**) The distribution of total Cac intensity across RP3 motorneuron active zones (n=3067 active zones (2 data points are outside the x-axis limits shown) from 16 NMJs of 4 animals). (**C**) The distribution of peak Cac intensity across RP3 motorneuron active zones (n=3067 active zones from 16 NMJs of 4 animals).

Figure 4

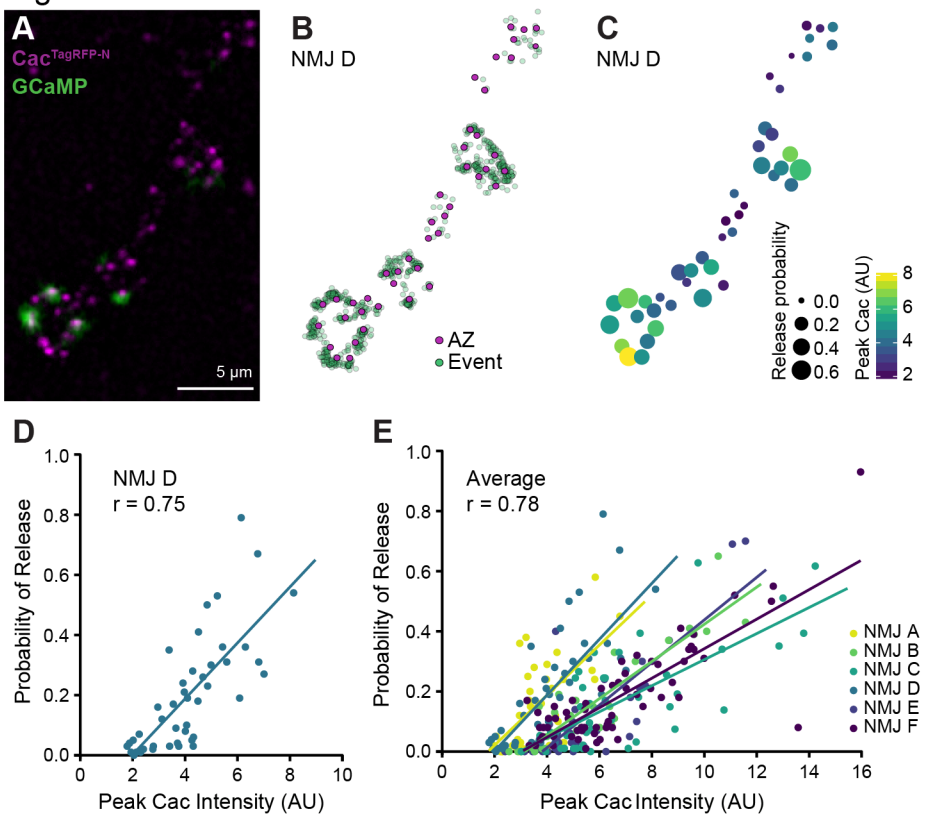

Figure 4. Calcium channel levels predict P_r at individual active zones of single motorneurons. (**A**) Confocal Z-projection of Cac in an RP3 motorneuron branch synapsing with muscle 6 in a live *cac*$^{TagRFP\text{-}N}$; PS-GCaMP preparation superimposed on a single background subtracted stimulation frame from a GCaMP movie. (**B**) Schematic of release events detected by postsynaptic GCaMP (green dots) during 1-Hz stimulation mapped to individual active zones marked by Cac$^{TagRFP\text{-}N}$ (magenta dots). (**C**) Heat map indicating P_r by size and Cac intensity by color. (**D**) Correlation between Cac and P_r at NMJ D (shown in A-C) (Pearson correlation (r)=0.75, n=44 active zones). (**E**) Correlation between Cac and P_r at six NMJs in six larvae (average Pearson correlation (r)=0.78).

Figure 5

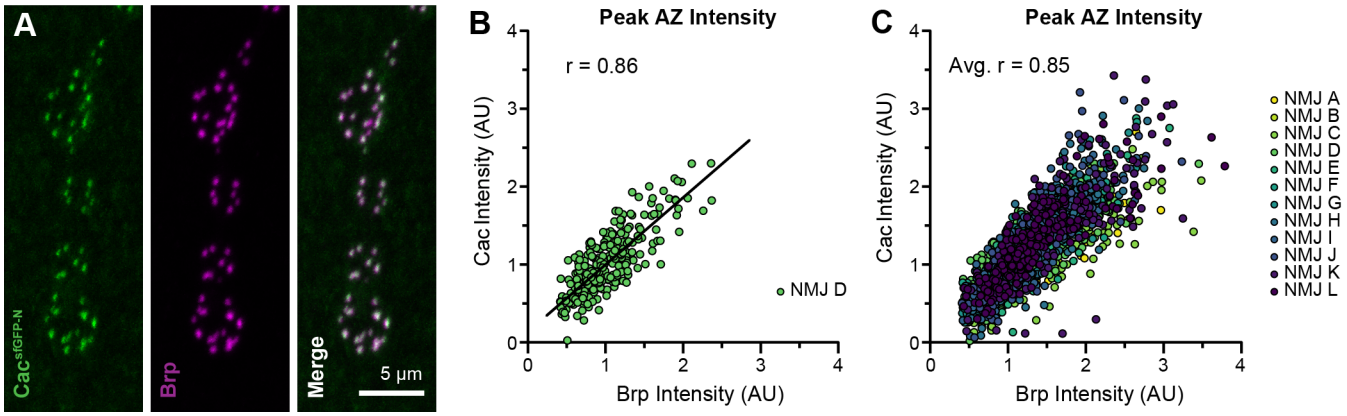

Figure 5. Cacophony and Bruchpilot levels are highly correlated at single synapses. (**A**) Confocal Z-projections of a *cac*$^{sfGFP\text{-}N}$ RP3 motorneuron branch co-labeled with antibodies against GFP and Brp. (**B**) Correlation between Cac and Brp peak active zone intensities at a single NMJ (Pearson correlation (r)=0.86, n=275 active zones from one NMJ). (**C**) Correlation between Cac and Brp peak active zone intensities (Pearson correlation (r)=0.85, n=12 NMJs from 4 animals).

Figure 6

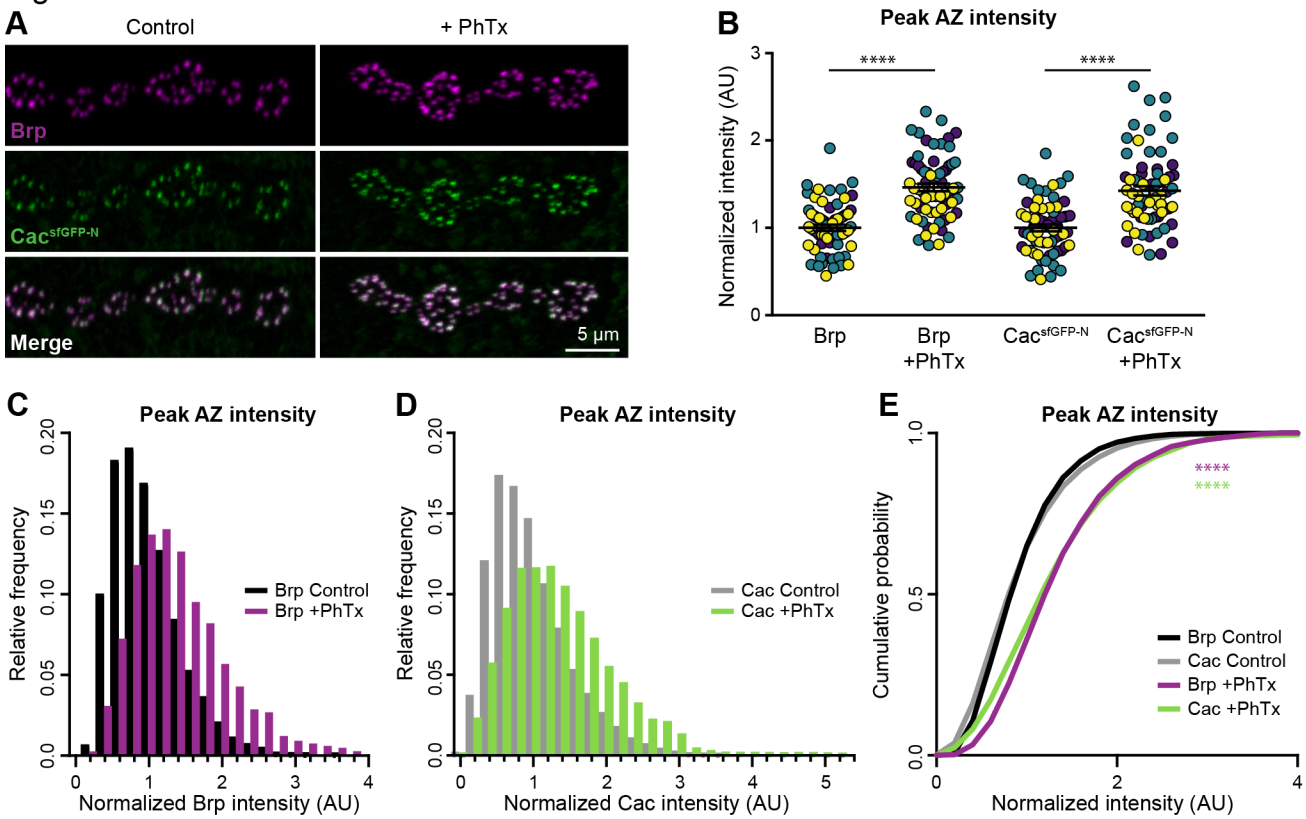

Figure 6. Cacophony levels are rapidly upregulated during acute homeostatic challenge. (**A**) Confocal Z-projections of *cac*$^{sfGFP\text{-}N}$ RP3 motorneuron boutons co-labeled with antibodies against GFP and Brp following vehicle (control) and PhTx treatment. (**B**) Normalized peak intensity of Brp and Cac per AZ averaged for each NMJ following 10-minute vehicle or PhTx treatment from three independent experiments signified by yellow, green, and purple symbols (Brp, 1.00 ± 0.04, n=65 NMJs from 18 larvae; Brp+PhTx, 1.46 ± 0.04, n=68 NMJs from 18 larvae, p<0.0001, Student's t test; *cac*$^{sfGFP\text{-}N}$, 1.00 ± 0.04, n=65 NMJs from 18 larvae; *cac*$^{sfGFP\text{-}N}$+PhTx, 1.42 ± 0.05, n=68 NMJs from 18 larvae, p<0.0001, Mann-Whitney U test). (**C**,**D**) Frequency distributions of peak Cac and Brp intensities at individual active zones of control and PhTx-treated animals reveal a rightward shift in intensities. (**E**) Cumulative probability distributions of Cac and Brp peak intensities in control and PhTx-treated animals (control, n=13,906 active zones; PhTx, n=16,007 active zones (28 data points are outside the x-axis limits shown), p<0.0001, Kolmogorov-Smirnov test).

Figure 7

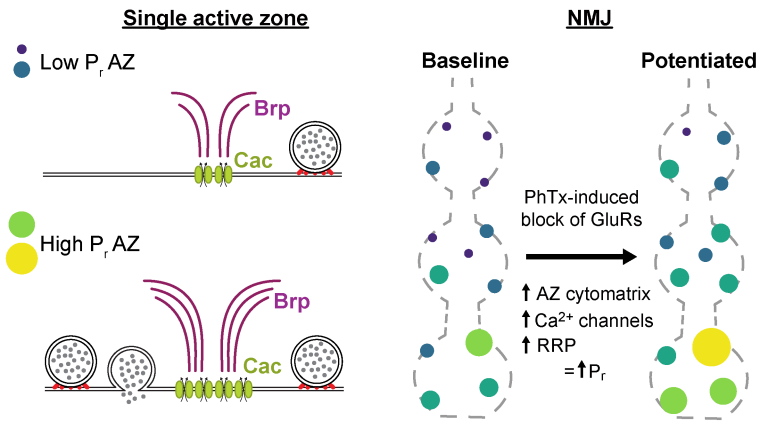

Figure 7. Calcium channel levels correlate with P_r and are rapidly upregulated during acute presynaptic homeostasis. High-P_r active zones have larger cytomatrices and localize more Cac compared to low-P_r active zones. When glutamate receptors are blocked by PhTx, active zones are rapidly remodeled to increase both the readily-releasable pool (RRP) of vesicles and calcium channel number, resulting in an overall increase in P_r.